Original Article

A pilot study of native T1-mapping for focal pulmonary lesions in 3.0 T magnetic resonance imaging: size estimation and differential diagnosis

Shuyi Yang[1#], Fei Shan[1#], Qinqin Yan[1], Jie Shen[1], Peiyan Ye[2], Zhiyong Zhang[1,3], Yuxin Shi[1], Rengyin Zhang[1]

[1]Department of Radiology, [2]Department of Hepatopathy, Shanghai Public Health Clinical Center, Fudan University, Shanghai 201508, China; [3]Fudan University, Shanghai 200433, China

Contributions: (I) Conception and design: S Yang, F Shan, Z Zhang, Y Shi; (II) Administrative support: Z Zhang, Y Shi; (III) Provision of study materials or patients: S Yang, Q Yan, F Shan, Z Zhang, Y Shi; (IV) Collection and assembly of data: S Yang, Q Yan, J Shen, P Ye, R Zhang; (V) Data analysis and interpretation: S Yang, F Shan, Q Yan, J Shen, P Ye, R Zhang; (VI) Manuscript writing: All authors; (VII) Final approval of manuscript: All authors.

[#]These authors contributed equally to this work.

Correspondence to: Zhiyong Zhang. Fudan University, Shanghai 200433, China. Email: zhyzhang@fudan.edu.cn; Yuxin Shi. Shanghai Public Health Clinical Center, Fudan University, Shanghai 201508, China. Email: shiyx828288@163.com.

Background: To investigate the accuracy of size estimation and potential diagnosis efficacy of native T1-mapping in focal pulmonary lesion, compared to T1-star 3D-volumetric interpolated breath-hold sequence (VIBE), T2-fBLADE turbo-spin echo (TSE), and computed tomography (CT).

Methods: Thirty-nine patients with CT-detected focal pulmonary lesions underwent thoracic 3.0-T magnetic resonance imaging (MRI) using axial free-breathing 3D T1-star VIBE, respiratory triggered T2-fBLADE TSE, breath-hold T1-Turbo fast low angle shot (FLASH) and T1-FLASH 3D. Native T1-mapping images were generated by T1-FLASH 3D with B1-filed correction by T1-Turbo FLASH. The intraclass correlation coefficient (ICC) and Bland-Altman plots were used to evaluate intra-observer agreement and inter-method reliability of diameter measurements. Native T1-values were measured and compared among the malignancy, tuberculosis, non-tuberculosis benign groups using Mann-Whitney U tests.

Results: Forty-five focal pulmonary lesions were displayed by CT, native T1-mapping, T1-star VIBE, and T2-fBLADE TSE. T1-mapping-based diameter measurements yielded an intra-observer ICC of 0.995. Additionally, inter-method measurements were highly consistent (T1-mapping & T1-star VIBE: ICC 0.982, T1-mapping & T2-fBLADE TSE: ICC 0.978, T1-mapping & CT: ICC 0.972). For lesions <3.00 cm, T1-mapping intra-observer (ICC 0.982) and inter-method diameter measurements were also highly consistent (T1-mapping & CT: ICC 0.823). Native T1-values of malignant tumors were lower than those of the non-tuberculosis benign lesions (P=0.003). Native T1-values of tuberculosis were lower than those of the non-tuberculosis benign lesions (P=0.002). Native T1-values showed no statistically significant differences between malignant tumors and tuberculosis (P=0.059).

Conclusions: Native T1-mapping enable accurate and reliable diameter measurement. Native T1-values potentially differentiate malignant tumors or tuberculosis from non-tuberculosis benign lesions.

Keywords: Pulmonary cancer; pulmonary tuberculosis; magnetic resonance imaging (MRI); T1-mapping

Submitted Nov 19, 2019. Accepted for publication Feb 24, 2020.
doi: 10.21037/jtd.2020.03.42
View this article at: http://dx.doi.org/10.21037/jtd.2020.03.42

Introduction

With advances in multi-detector computed tomography (MDCT), increasing numbers of pulmonary nodules have been detected incidentally, which are of concern to patients and clinicians due to the probability of malignance, as well as pulmonary mass which can be malignant tumors or consolidation due to infection. There have been numerous studies of the early detection and evaluation of focal pulmonary lesions by various radiologic approaches, including CT and magnetic resonance imaging (MRI), with promising results (1-5). In addition, nodule type and size assessments are considered effective biomarkers for nodule management to reduce lung cancer-specific mortality, according to the recommendation by the Fleischner Society and the findings reported by the Lung Cancer Screening Committee for the American College of Radiology (6,7). CT is currently considered to be the gold standard for the detection and morphological evaluation of focal pulmonary lesions and is the predominant approach for follow-up examinations in lesions management; this leads to a high cumulative radiation exposure.

Advances in MRI, including high-performance gradients, phased-array receiver coils, parallel imaging, refined imaging sequences, and high-field MRI systems, allow application of this modality in routine clinical practice (8). Recent studies have demonstrated its capability for pulmonary disease assessment, including focal and diffuse pulmonary lesions (4,9-11). In a review, Ohno *et al.* concluded that state-of-the-art thoracic MRI was now a substitute for traditional radiological examinations and played a complementary role in the management of patients with various pulmonary disease, especially those with focal pulmonary lesions (12). Thoracic MRI with ultrashort echo time as well as Short-tau inversion recovery (STIR) T2-weighted turbo-spin echo (TSE) imaging would be better for focal pulmonary lesion detection in routine clinical practice, while the lesion detection capability of 3D T1-weighted gradient echo volumetric interpolated breath-hold examination (VIBE) sequence is lower than that of TSE imaging (3,12). The VIBE sequence with radial acquisition trajectory by stack-of star (star-VIBE) and TSE with fast-BLADE (fBLADE), which also named periodically rotated overlapping parallel lines with enhanced reconstruction (PROPELLER), are insensitive to motion and magnetic susceptibility artifacts, which can improve the image quality (13,14).

Water proton longitudinal relaxation time (T1) of lung lesions can provide important information for regional characterization of pulmonary diseases. Previous studies on this topic focused on functional assessment in chronic obstructive pulmonary disease (COPD) (15,16). T1-mapping, as a quantitative MRI technique with short scanning time, may be able to evaluate the focal pulmonary lesions by depicting lesions clearly and calculating lesions T1-values. The ideal MRI sequence that can be considered as a potential alternative to CT for assessment of pulmonary lesions should achieve sufficient accuracy for display and size estimation of lesions, as well as, provide more information for differential diagnosis.

In this study, we investigated whether native T1-mapping could depict focal pulmonary lesions clearly, with highly accurate size estimation, as compared to T1-star VIBE and T2-fBLADE TSE, as well as CT, which regarded as the gold standard. We also expected that native T1-values were conducive to differentiate pulmonary malignant tumors from benign lesions.

Methods

Patients

The review board of Shanghai Public Health Clinical Center, Fudan University approved the protocol of this study and written informed consent was obtained from each patient (Ethic ID: 2019-S021-02).

Fifty-five consecutive patients with focal pulmonary lesions detected by CT were advised to undergo dedicated thoracic MRI between November 2018 and February 2019. The inclusion criteria were as follows: (I) focal pulmonary lesions larger than 10mm in maximum diameter and manifested as part-solid or solid lesions by CT; (II) without contraindication for MR imaging, including pacemaker, ferromagnetic implants, claustrophobia, etc. The exclusion criteria were as follows: (I) patients with severely impaired pulmonary function, such as acute exacerbated COPD, interstitial pneumonia, etc.; (II) patients without excellent coordination (lower breath-hold capability and compliance), with larger motion artifact. The workflow of the study is demonstrated in *Figure 1*. Finally, thirty-nine patients (male:female, 29:10; median age, 64 years; age range, 20–84 years) were enrolled in this study. All patients achieved clinical diagnosis by pathological results from operations/biopsies or received anti-inflammatory therapies with perfect cure outcome. The interval between thoracic MRI

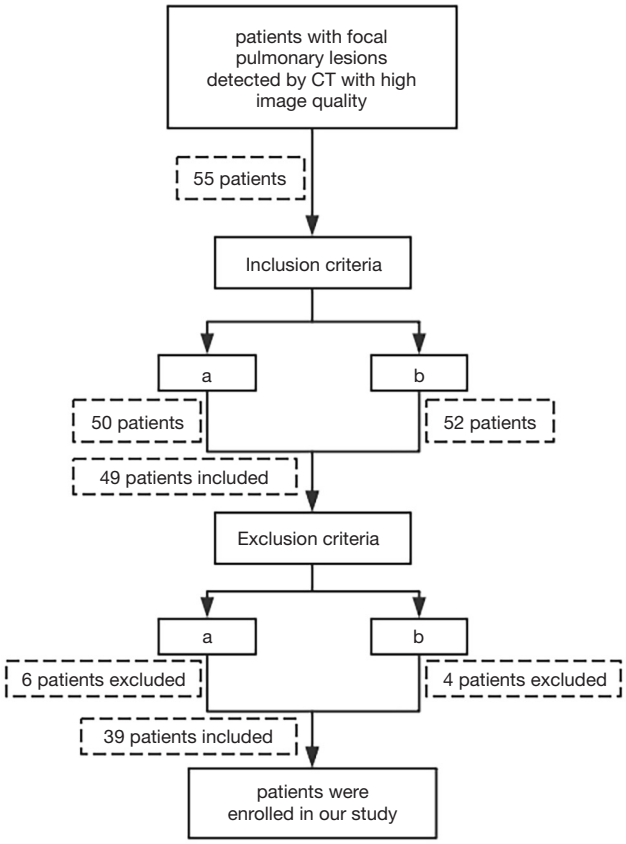

Figure 1 The workflow of the study. Inclusion criteria: (a) focal pulmonary lesions larger than 10 mm in maximum diameter and manifested as part-solid or solid lesions by computed tomography, (b) without contraindication for magnetic resonance imaging, including pacemaker, ferromagnetic implants, claustrophobia, etc. Exclusion criteria: (a) patients with severe pulmonary diseases, such as chronic obstructive pulmonary diseases (COPD), interstitial pneumonia, etc., (b) patients lacking cooperation, with larger motion artifact.

and CT was less than 3 days (mean, 1.2 days).

MR imaging

All patients underwent 3.0-T MRI (MAGNETOM Skyra, Siemens Healthcare, Erlangen, Germany) with a 32-channel body-phased array coil. The MRI sequences were as follows (*Table 1*): axial free-breathing T1-star VIBE (TR/TE 2.79/1.39 ms, slice-thickness 3.00 mm, base resolution 320, scanning time 103 seconds), with spectrally selective attenuated inversion recovery, axial respiratory triggered (RT) T2-fBLADE TSE (TR/TE 1,870.00/69.00 ms, slice thickness 3.00 mm, base resolution 320, scanning time 383 seconds) with STIR, axial breath-hold (BH) T1-Turbo fast low angle shot (FLASH) (TR/TE 5,320.00/ 2.06 ms, slice thickness 4.00 mm, base resolution 64, scanning time 11 seconds) and T1-FLASH 3D (TR/TE 5.01/2.30 ms, slice thickness 4.00 mm, flip angles 3/15 deg, base resolution 224, scanning time 14 seconds). For BH sequences, the examinations were performed with respiratory surveillance using a respiratory belt. Native T1-mapping images were generated by T1-FLASH 3D. To increase the accuracy, a B1-filed correction sequence (T1-Turbo FLASH) was added before T1-mapping. The T1-mapping pseudocolor map was automatically calculated and generated.

CT imaging

All patients underwent conventional thoracic CT examinations with the 320-detector system (Aquilion Vision, Canon Medical Systems, Japan) at full inspiration. Scanning range was from the level of the thoracic inlet to the inferior level of the costophrenic angle. The

Table 1 Imaging parameters for MRI sequences performed at 3.0 Tesla

Parameter	Axial free-breathing T1-star VIBE	Axial RT T2-fBLADE TSE	Axial BH T1-turbo FLASH	Axial BH T1-FLASH 3D
TR (ms)	2.79	1,870.00	5,320.00	5.01
TE (ms)	1.39	69.00	2.06	2.30
Slice thickness (mm)	3	3	4	4
Base resolution	320	320	64	224
Scanning time (s)	103	383	11	14
Fat suppression	SPAIR	STIR	–	–

MRI, magnetic resonance imaging; RT, respiratory triggered; BH, breath-hold; VIBE, volumetric interpolated breath-hold examination; SPAIR, spectrally selective attenuated inversion recovery; STIR, short-tau inversion recovery; FLASH, fast low angle shot.

scanning protocols were as follows: detector width, 80×0.5 mm; pitch, 0.813; tube voltage, 120 kV; automatic tube current with SD 10 (Sure Exp 3D set, maximum: 440 mA, minimum: 60 mA). The radiation dose of the thoracic CT was calculated in terms of the dose-length product (DLP). An effective radiation dose was calculated by a formula as DLP × conversion factor (0.017 $mSv \cdot mGy^{-1}\ cm^{-1}$ for the chest). Average radiation dose was 5.22 mSv. All CT images with 1 mm contiguous section thickness were reconstructed by means of adaptive iterative dose-reduction with three-dimensional processing (AIDR 3D, standard) and a high frequency reconstruction algorithm (FC56) for the lung window setting, and with a standard reconstruction algorithm (FC17) for the mediastinum window setting. The lung window width and level were adjusted appropriately by the reference standards of 1,600 and –600 Hounsfield unit (Hu). Nonionic iodinated contrast agent (60–80 mL iohexol 350 mgI/mL, Beilu Pharmaceutical Co., Ltd.; Beijing, China) was injected from cubital vein at the dose of 3 mL/s in 13 patients.

Image analysis

MRI and CT images were all reviewed with the same picture archiving and communication system, while the native T1-mapping pseudocolor maps were evaluated on the Master workstation (Siemens Healthcare, Erlangen, Germany). A board-certified chest radiologist with 17 years' experience in CT and MRI scan interpretation, blindly evaluated pulmonary lesions using MRI images (native T1-mapping, T1-star VIBE and T2-fBLADE TSE) and CT images obtained at different times on different days. To mitigate potential recall bias, the interval between reading native T1-mapping, T1-star VIBE, T2-fBLADE TSE and CT images were more than 2 weeks, while the interval between reading native T1-mapping twice were more than 1 month. The lesions location, size and other vital imaging features were recorded. The size of the lesions was recorded as maximum diameter in axial images with excellent lesion delineation. To measure focal pulmonary lesions' native T1-value accurately, the region of interest (ROI) was manually drawn on the solid part of the lesion at the level of maximum transverse diameter, avoiding necrosis, hemorrhage, bronchus and big vessels blinded to the pathologic results.

Statistical analysis

Statistical analyses were performed using MedCalc 18.11.3 (MedCalc Software bvba, Ostend, Belgium) software packages. Since some patients had more than one pulmonary lesion, a per-lesion based approach was used for data analysis. Descriptive analysis was used for lesion location and size. All continuous variables were presented as median and standard deviation, while categorical variables were shown as percentage. The intraclass correlation coefficient (ICC) and Bland-Altman method were used to evaluate the intra-observer agreement of diameter measurements and to test the consistence of diameter measurements between native T1-mapping and other radiologic methods (T1-star VIBE, T2-fBLADE and CT). As the ICC approached 1, the intra-observer agreement or the diameter measurement consistency between the tested methods was better (excellent: >0.75, mild: 0.40< ICC ≤0.74, poor ≤0.40). In Bland-Altman plot, the mean maximum diameters of lesions measured by the two target methods were plotted along the horizontal axis and the difference in the value between the two methods was plotted along the vertical axis. Native T1-values of malignant tumors and benign groups were compared by Mann-Whitney U test. The test was two-tailed, and $P<0.05$ was considered statistically significant.

Results

A total of 45 pulmonary lesions, measuring from 1.00 to 7.80 cm (3.30±1.90 cm) were identified by CT, in 39 patients. Of these, 24 lesions (53.33%) were in the right lung and 21 (46.67%) in the left lung (*Table 2*). There were 27 pulmonary lesions <3.00 cm according to CT, ranging from 1.00 to 2.92 cm in size.

The clinical diagnosis revealed 25 and 20 cases of malignant tumors and benign lesions, respectively. The malignancy group included 11 adenocarcinomas, 7 squamous cell carcinomas and 7 metastatic tumors (2 from cervical cancer, 5 from lung cancer). The benign lesions included 7 tuberculosis and 13 non-tuberculosis benign lesions (3 fungal infection, 6 inflammatory hyperplasia and 4 spherical pneumonia) (*Table 2*).

Lesion display

Native T1-mapping displayed all the lesions, as did T1-starVIBE and T2-fBLADE TSE. Four lesions were shown as consolidation by non-contrast enhanced CT, with the obscure boundaries to the adjacent obstructive pulmonary atelectasis and/or pneumonia, but the boundaries were demonstrated clearly in the native T1 pseudocolor map

Table 2 Lesions characteristics

Characteristics	All (N=39/n=45)*
Gender	39
Male	29
Female	10
Size	45
≤3 cm	27
>3 cm	18
Right lung	24
Upper lobe	10
Middle lobe	5
Lower lobe	9
Left lung	21
Upper lobe	15
Lower lobe	6
Benign	20
Tuberculosis	7
Fungal infection	3
Inflammatory hyperplasia	6
Spherical pneumonia	4
Malignancy	25
Adenocarcinoma	11
Squamous cell carcinoma	7
Metastatic tumor	7

*, N represents for the number of patients, n represents for the number of lesions.

(*Figure 2*). The tumor showed a blue zone with an adjacent red zone in the pseudocolor map. Native T1-mapping clearly depicted pulmonary lesion as well as thrombus in the right pulmonary artery (*Figure 2*). The color of pulmonary metastatic tumors was shown in a different color. A part-solid nodule with a maximum diameter of 1.1 cm (consolidation portion diameter: 0.7 cm) (*Figure 3*) and nodules with the tree-in-bud sign (*Figure 4*) were also displayed with T1-mapping.

Lesion size analysis

The maximum diameter of the lesions was measured twice by a chest radiologist on native T1-mapping, with an interval of more than 1 month. The mean diameters obtained during these measurements were 3.40±1.95 and 3.43±2.02 cm, indicating excellent intra-observer agreement (ICC: 0.995, 95% CI: 0.992–0.998; Bland-Altman method: mean difference –0.03 cm), while for lesions smaller than 3.00 cm, the results were 2.14±0.58 and 2.14±0.58 cm, also indicating excellent intra-observer agreement (ICC: 0.982, 95% CI: 0.961–0.992; Bland-Altman method: mean difference 0.01 cm).

The maximum diameter of the lesions measured by T1-star VIBE, T2-fBLADE TSE, and CT, were 3.17±1.94, 3.24±1.92, and 3.30±1.90 cm, respectively. The maximum lesion diameter measured by T1-mapping achieved excellent inter-methods consistency (*Table 3*; *Figure 5*). For lesions smaller than 3.00 cm, the consistency of lesion diameter measured by T1-mapping and CT was also excellent, with an ICC value of 0.823 and 95% CI value of 0.787–0.956 (*Table 3*).

Native T1-values of lesions

Native T1-values of these focal pulmonary lesions were shown in *Table 4* and *Figure 6*. Native T1-values of malignant tumors were lower than those of non-tuberculosis benign lesions (1,454.19±349.92 and 2,019.49±516.55 ms, P=0.003). Native T1-values of tuberculosis were lower than those of non-tuberculosis benign lesions (1,195.60±263.65 and 2,019.49±516.55 ms, P=0.002). The difference of native T1-values between malignant tumors and tuberculosis was not statistically different (1,454.19±349.92 and 1,195.60±263.65 ms, P=0.059).

Discussion

To the best of our knowledge, there have been no previous studies assessing the display or evaluation of focal pulmonary diseases by native T1-mapping, even though this quantitative MRI approach with short scanning time could potentially reduce radiation exposure of patients with pulmonary lesions. CT is the gold standard of pulmonary lesions diagnosis, while T1-star VIBE and T2-fBLADE TSE are routine sequences with new techniques in thoracic MRI scanning. Here, we showed that native T1-mapping demonstrates focal pulmonary lesions clearly and enabled accurate and reliable diameter measurement, compared to T1-star VIBE, T2-fBLADE TSE and CT. Native T1-values were potentially conducive to differentiate malignant tumors or tuberculosis from non-tuberculosis benign lesions.

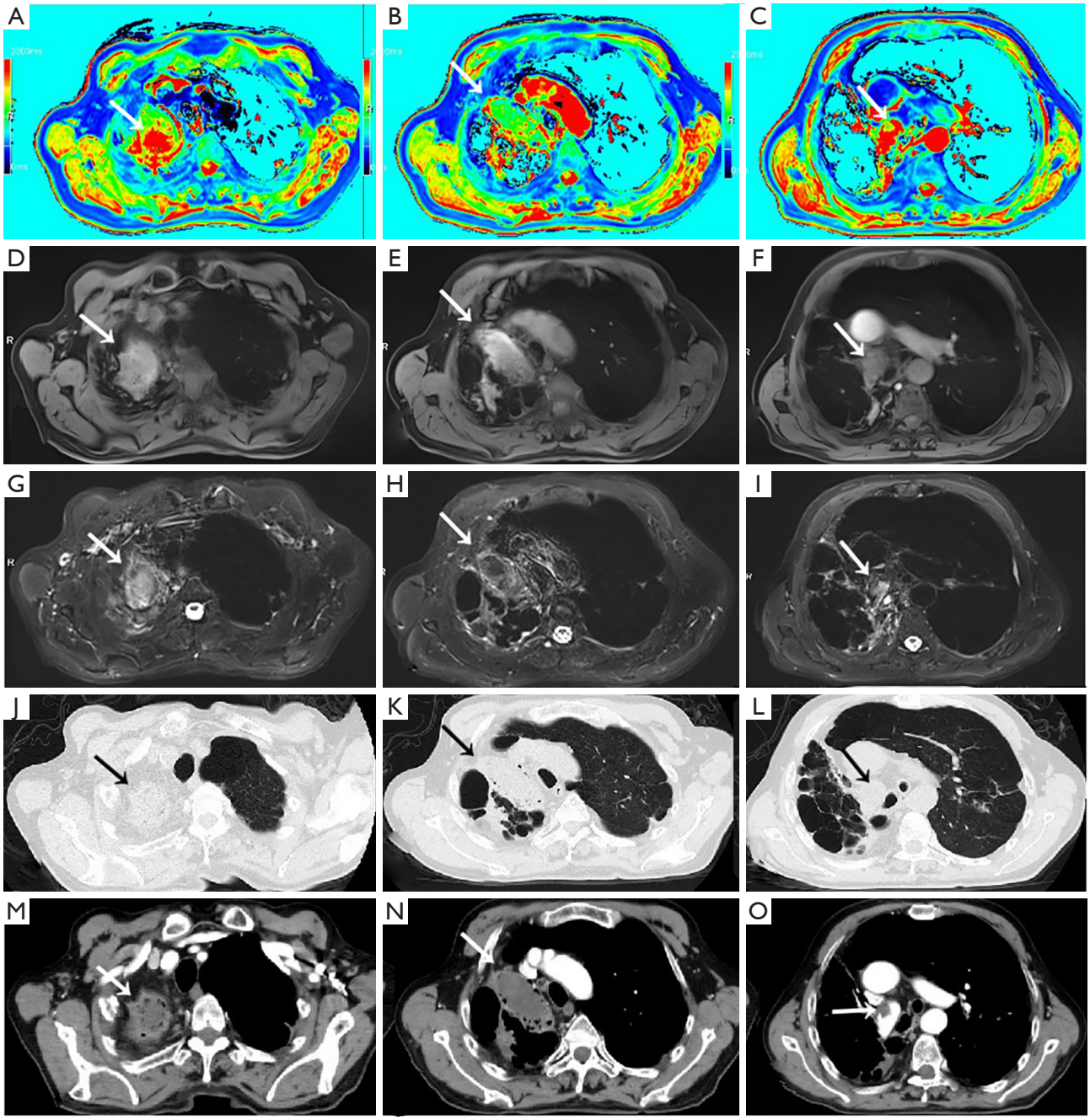

Figure 2 A patient with chronic lung tuberculoma and peripheral active infection. (A,B,C) Native T1-mapping qseudocolor map, (D,E,F) T1-Star VIBE, (G,H,I) T2-fBLADE TSE, (J,K,L) computed tomography (CT; lung window), (M,N,O) CT, mediastinal window, contrast-enhancement. The lesion in the right superior lobe (K/N, '→') was manifested more intensely in T1-starvibe (E, '→') and less intensely in T2-fBLADE TSE (H, '→'). T1-mapping shows the lesion clearly (B, '→'). The peripheral active infection (J/M, '→') manifested less intensely in T1-star VIBE (D, '→') but more intensely in T2-fBLADE (G, '→'). T1-mapping shows the infection clearly, manifested as a red zone (A, '→'). The thrombus in the right pulmonary artery, confirmed by enhanced CT (O, '→') can also be detected by native T1-mapping (C, '→') and T2-fBLADE (I, '→'), but could not be seen in T1-star VIBE (F, '→') and CT (lung window, L, '→'). Due to the difference of the flow velocity and direction in the aorta, the signal intense was nonuniform with the flowing void effect in the ascending aorta. VIBE, volumetric interpolated breath-hold examination; TSE, turbo-spin echo.

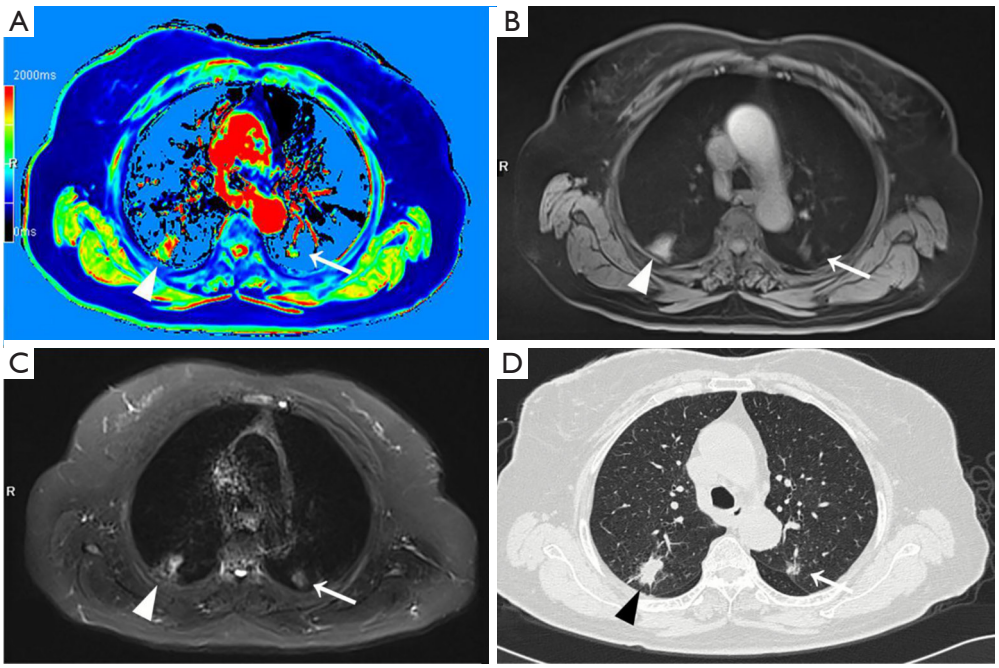

Figure 3 A patient with two simultaneous primary lung adenocarcinomas. (A) Native T1-mapping qseudocolor map; (B) T1-star VIBE; (C) T2-fBLADE; (D) computed tomography (CT; lung window). A nodule in the left superior lobe can be detected clearly by T1-mapping (A, white '→') while manifested as a part-solid nodule in CT (D, white '→'). The part-solid nodule was less intense in T1-star VIBE (B, white '→'), but more intense in T2-fBLADE TSE (C, white '→'). Another solid nodule, located in the right superior lobe (D, black ' △ '), can also be clearly detected by T1-mapping (A, white ' △ '). The nodule was slightly more intense in T1-star VIBE (B, white ' △ '), and markedly more intense in T2-fBLADE TSE (C, white ' △ '). VIBE, volumetric interpolated breath-hold examination; TSE, turbo-spin echo.

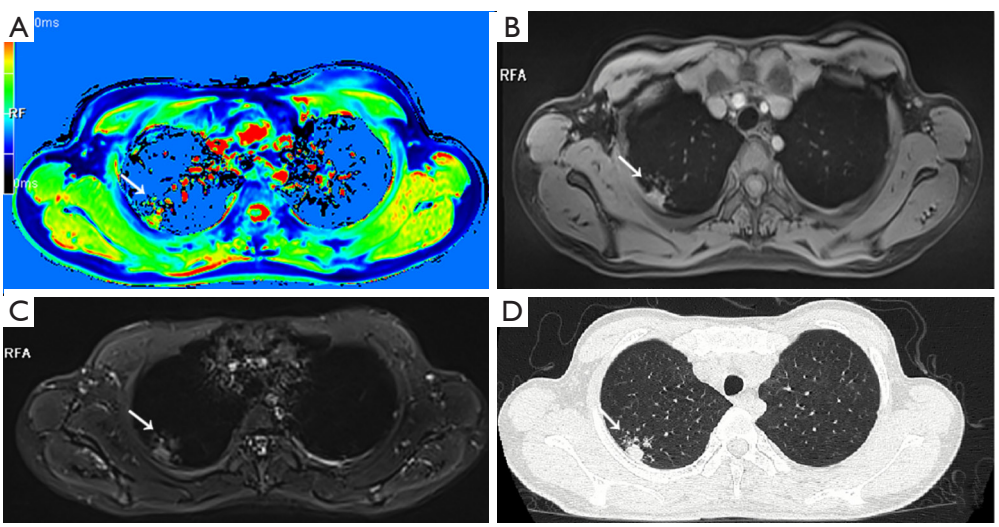

Figure 4 A pulmonary tuberculosis (TB) patient with lesions in the right superior lobe. (A) T1-mapping qseudocolor map; (B) T1-star VIBE; (C) T2-fBLADE; (D) computed tomography (CT; lung window). A TB lesion with the tree-in-bud sign (D, white '→') , located in the right superior lobe, can be clearly detected by T1-mapping (A, white '→'). The lesion was slightly more intense in T1-star VIBE (B, white '→'), and T2-fBLADE (C, white '→'). VIBE, volumetric interpolated breath-hold examination.

Table 3 The agreement and consistence analysis of lesions size

Radiologic examinations	Mean difference (cm)	95% LA (cm)	RC	ICC	95% CI
T1 mapping#1 & T1 mapping#2	–0.03	–0.40 to 0.34	0.372	0.995	0.992–0.998
T1 mapping#1 & T1-star VIBE	0.23	–0.49 to 0.95	–	0.982	0.968–0.990
T1 mapping#1 & T2-fBLADE TSE	0.17	–0.63 to 0.96	–	0.978	0.961–0.988
T1 mapping#1 & CT	0.15	–0.75 to 1.05	–	0.972	0.950–0.985
T1 mapping#1 & T1 mapping#2*	0.01	–0.21 to 0.22	0.213	0.982	0.961–0.992
T1 mapping#1 & CT*	0.10	–0.55 to 0.75	–	0.823	0.787–0.956

#1: measured firstly; #2: measured secondly; *, lesions smaller than 3.00 cm by CT. VIBE, volumetric interpolated breath-hold examination; TSE, turbo-spin echo; LA, limits of agreement; RC, repeatability coefficient; ICC, intraclass correlation coefficient; CI, confidence interval.

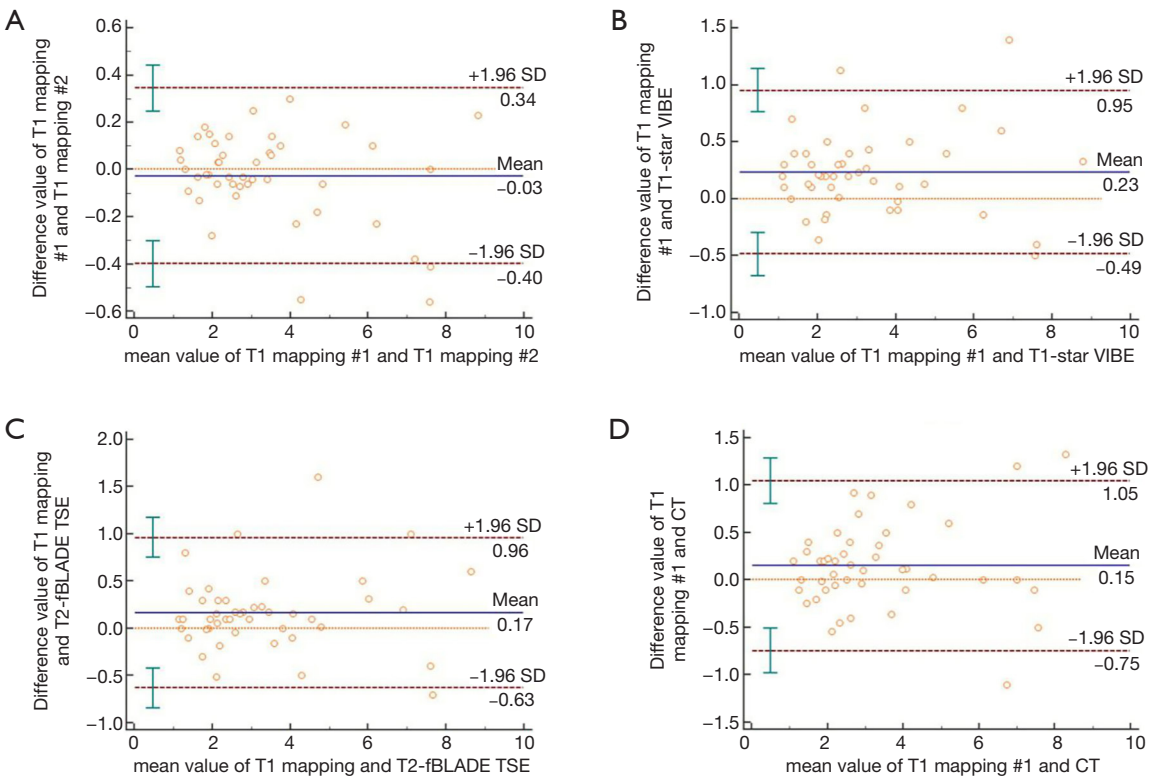

Figure 5 Bland-Altman plot. The mean difference in tumor diameters determined with different methods is indicated by the solid line. The two outer dotted lines represent the 95% limits of agreement (95% LA). The diameter measurement consistency of T1 mapping twice, T1 mapping and T1-star VIBE, T1 mapping and T2-fBLADE TSE, T1 mapping and CT, was acceptable. VIBE, volumetric interpolated breath-hold examination; TSE, turbo-spin echo.

T1-mapping has been widely used and studied in the field of myocardiopathy (17-19), liver disease (20,21), brain tumors (22), and some other organ diseases (23-25). T1-relaxation time is a potential imaging biomarker in lung disease (26). T1 mapping is defined by the pixel-to-pixel illustration of absolute T1 relaxation times and enabling a reliable T1 quantification, directly reflecting underlying pathophysiological processes (24). Different lesions or the same lesions at different stages may have different T1-relaxation times due to the difference in water content, which can be depicted by different color gradations in a pseudocolor map derived by native T1-

Table 4 Native T1-value of focal pulmonary lesions

Lesions	n	Minimum (ms)	Maximum (ms)	Average (ms)	Standard deviation (ms)
Malignancy	25	799.70	2,111.65	1,454.19	349.92
Tuberculosis	7	934.70	1,702.95	1,195.60	263.65
Non-tuberculosis benign lesions	13	1,190.10	2,772.05	2,019.49	516.55

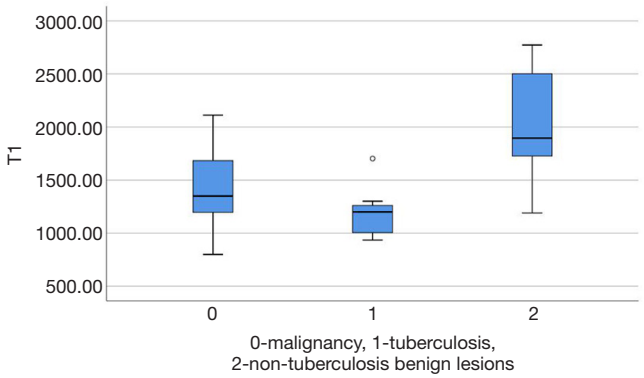

Figure 6 The box-type diagram for T1 values of pulmonary malignant tumors, pulmonary tuberculosis and non-tuberculosis benign lesions.

mapping (17-26). The T1-relaxation time of pulmonary lesions also differs from that of the pulmonary parenchyma, which may promote the detection capability of pulmonary lesions. In our study, the tumors with the adjacent obstructive atelectasis or pneumonia were clearly detected in the pseudocolor map, due to different T1-relaxation times between lesions. A part-solid nodule measured 1.1 cm (consolidation portion diameter: 0.7 cm) and the micronodules were seen as a tree-in-bud sign on native T1-mapping, which indicated its potential application for nodule detection with shorter scanning time than the routine scanning sequences (T1-star VIBE and T2-fBLADE TSE). Native T1-mapping can also evaluate endovascular lesions, which have different T1-relaxation times as compared with blood.

As a potential substitute to follow-up CT, thoracic MRI should allow accurate lesion measurement (6,7). In our study, lesion size estimation by native T1-mapping yielded excellent intra-observer agreement and inter-method consistency. In Bland-Altman plots (*Figure 5D*), the dots plotted away from the 95% LA mainly represented lesions larger than 6 cm, which might represent tumors with obstructive pulmonary atelectasis and pneumonia. On non-enhanced CT, it was difficult to identify these tumors clearly from the adjacent lesions, which might reduce the accuracy of lesion size measurement. For lesions smaller than 3 cm, the consistency of lesion diameter measurements obtained by T1-mapping and by CT was excellent (ICC: 0.823, 95% CI: 0.787–0.956; mean difference: 0.10 cm, 95% CI: –0.55 to 0.75), which indicated that T1-mapping could be a new method for follow-up of focal pulmonary lesions.

T1-mapping, as a quantitative MRI technique, can also quantify T1-values of tissues accurately. In our study, native T1-values of malignant tumors were significantly lower than those of non-tuberculosis benign lesions, such as fungal infection, inflammatory hyperplasia and spherical pneumonia. The pathological change of pulmonary parenchyma, such as inflammation, leading to an increased T1 relaxation time, may due to the increase of water content (24). We considered that pulmonary tuberculosis with caseous necrosis achieved lower T1-values due to the lower content of water content, which resulted in the good differentiate diagnosis efficacy of T1-values from non-tuberculosis lesions but bad efficacy from malignant tumors (water content lower than inflammation). The variations of T1-value between pre- and post-contrast-enhanced T1-mapping reflected micro-circulation in lesions, which could also be a significant biomarker for lesions diagnosis (23,24).

We also compared the lesions size estimation by native T1-mapping to the routine thoracic MRI sequences with new techniques (free-breathing T1-star VIBE and RT T2-fBLADE TSE), which would be described blow. The focal pulmonary lesions detection capability by T1-VIBE had been reported to range from 54.1% (lesion diameter range, 1–31 mm) to 87.3% (lesion diameter range, 1–61 mm) (3,12,27,28). Free-breathing T1-star VIBE using radial k-space data sampling substantially reduced motion-related artifacts and could compensate for breathing, heart pulsation, and other motion artifacts, providing high-resolution imaging and promoting image quality (29-32). Compared to the traditional T1-VIBE, T1-star VIBE is useful for displaying the morphological characteristics of peripheral solid pulmonary masses under free-breathing

conditions, which is useful for patients that cannot comply with BH requirements (13,29).

T2-TSE has been recommended for focal pulmonary lesions detection in routine clinical practice, with a high lesion detection sensitivity (90.8%) (12,28), but the image quality is poor, due to the lower proton density and the respiratory and heart pulsation motion artifacts. PROPELLER acquires k-space data with rotating parallel lines instead of parallel lines can markedly reduce the occurrence of motion and magnetic susceptibility artifacts and can aid in visualizing small lesions, especially in patients who are not cooperative or who have physiologic motions (33). Compared to the TSE sequence, the BLADE technique can reduce respiratory motion, and heart and vascular pulsation artifacts, while decreasing the scanning time and improving the anatomic depiction and image quality (14). However, there are more radial artifacts with the BLADE sequence. The fBLADE is the upgraded version of BLADE, with a broader rotating line, which can reduce motion and magnetic susceptibility artifacts better, as well as decreasing the scanning time. In our study, all lesions were displayed by T1-star VIBE and T2-fBLADE TSE sequences. The consistency of lesion diameter measured by T1-mapping and T1-star VIBE, T2-fBLADE TSE, was also excellent (*Table 3*). The scan time of T1-mapping was several seconds, which was markedly shorter than that of T1-star VIBE and T2-fBLADE TSE; additionally, the T1-mapping pseudocolor map displayed the lesions more distinctly.

There are some limitations in our study. This is a pilot study to investigate the potential of native T1-mapping for assessing pulmonary lesions. The contrast-enhanced T1-mapping, which may be helpful in lesion diagnosis, is not investigated in this study. All the lesions were larger than 1.0 cm, while pure ground glass nodule was precluded in this pilot study. T1-star VIBE and T2-fBLADE TSE, as potential sequences for focal pulmonary lesions detection, have rarely been studied previously, and are used as reference sequences in this study. We will study lesion detection and diagnosis by these sequences in the near future.

Conclusions

Native T1-mapping, as a quantitative MRI technique, was shown to be able to depict pulmonary lesions clearly and allow accurate size estimation of the tumor, with excellent intra-observer agreement and inter-method agreement. The native T1-values of focal pulmonary lesions are potentially conducive to lesions diagnosis, especially for malignant tumors or tuberculosis with non-tuberculosis benign lesions.

Acknowledgments

Funding: Shanghai Municipal Science and Technology Commission, No. 18411967100.

Footnote

Conflicts of Interest: All authors have completed the ICMJE uniform disclosure form (available at http://dx.doi.org/10.21037/jtd.2020.03.42). The authors have no conflicts of interest to declare.

Ethical Statement: The authors are accountable for all aspects of the work in ensuring that questions related to the accuracy or integrity of any part of the work are appropriately investigated and resolved. The review board of Shanghai Public Health Clinical Center, Fudan University approved the protocol of this study and written informed consent was obtained from each patient (Ethic ID: 2019-S021-02).

References

1. National Lung Screening Trial Research Team, Aberle DR, Adams AM, et al. Reduced lung-cancer mortality with low-dose computed tomographic screening. N Engl J Med 2011;365:395-409.
2. Horeweg N, Scholten ET, de Jong PA, et al. Detection of lung cancer through low-dose CT screening (NELSON): a prespecified analysis of screening test performance and interval cancers. Lancet Oncol 2014;15:1342-50.
3. Allen BD, Schiebler ML, Sommer G, et al. Cost-effectiveness of lung MRI in lung cancer screening. Eur

Radiol 2020;30:1738-46.
4. Burris NS, Johnson KM, Larson PE, et al. Detection of Small Pulmonary Nodules with Ultrashort Echo Time Sequences in Oncology Patients by Using a PET/MR System. Radiology 2016;278:239-46.
5. Ruilong Z, Daohai X, Li G, et al. Diagnostic value of 18F-FDG-PET/CT for the evaluation of solitary pulmonary nodules: a systematic review and meta-analysis. Nucl Med Commun 2017;38:67-75.
6. Naidich DP, Bankier AA, MacMahon H, et al. Recommendations for the management of subsolid pulmonary nodules detected at CT: a statement from the Fleischner Society. Radiology 2013;266:304-17.
7. MacMahon H, Naidich DP, Goo JM, et al. Guidelines for Management of Incidental Pulmonary Nodules Detected on CT Images: From the Fleischner Society 2017. Radiology 2017;284:228-43.
8. Sieren JC, Ohno Y, Koyama H, et al. Recent technological and application developments in computed tomography and magnetic resonance imaging for improved pulmonary nodule detection and lung cancer staging. J Magn Reson Imaging 2010;32:1353-69.
9. Koyama H, Ohno Y, Seki S et al. Value of diffusion-weighted MR imaging using various parameters for assessment and characterization of solitary pulmonary nodules. Eur J Radiol 2015;84:509-15.
10. Lonzetti L, Zanon M, Pacini GS, et al. Magnetic resonance imaging of interstitial lung diseases: A state-of-the-art review. Respir Med 2019;155:79-85.
11. Ohno Y, Koyama H, Yoshikawa T, et al. T2* measurements of 3-T MRI with ultrashort TEs: capabilities of pulmonary function assessment and clinical stage classification in smokers. AJR Am J Roentgenol 2011;197:W279-85.
12. Ohno Y, Kauczor HU, Hatabu H, et al. MRI for solitary pulmonary nodule and mass assessment: Current state of the art. J Magn Reson Imaging 2018;47:1437-58.
13. Kumar S, Rai R, Stemmer A, et al. Feasibility of free breathing Lung MRI for Radiotherapy using non-Cartesian k-space acquisition schemes. Br J Radiol 2017;90:20170037.
14. Zhang L, Tian C, Wang P, et al. Comparative study of image quality between axial T2-weighted BLADE and turbo spin-echo MRI of the upper abdomen on 3.0 T. Jpn J Radiol 2015;33:585-90.
15. Alamidi DF, Morgan AR, Hubbard Cristinacce PL, et al. COPD Patients Have Short Lung Magnetic Resonance T1 Relaxation Time. COPD 2016;13:153-9.
16. Morgan AR, Parker GJ, Roberts C, et al. Feasibility assessment of using oxygen-enhanced magnetic resonance imaging for evaluating the effect of pharmacological treatment in COPD. Eur J Radiol 2014;83:2093-101.
17. Wan K, Li W, Sun J, et al. Regional amyloid distribution and impact on mortality in light-chain amyloidosis: a T1 mapping cardiac magnetic resonance study. Amyloid 2019;26:45-51.
18. Contti MM, Barbosa MF, Del Carmen Villanueva Mauricio A, et al. Kidney transplantation is associated with reduced myocardial fibrosis. A cardiovascular magnetic resonance study with native T1 mapping. J Cardiovasc Magn Reson 2019;21:21.
19. Taylor AJ, Salerno M, Dharmakumar R, et al. T1 Mapping: Basic Techniques and Clinical Applications. JACC Cardiovasc Imaging 2016;9:67-81.
20. Kim JE, Kim HO, Bae K, et al. T1 mapping for liver function evaluation in gadoxetic acid-enhanced MR imaging: comparison of look-locker inversion recovery and B1 inhomogeneity-corrected variable flip angle method. Eur Radiol 2019;29:3584-94.
21. Faller TL, Trotier AJ, Miraux S, et al. Radial MP2RAGE sequence for rapid 3D T1 mapping of mouse abdomen: application to hepatic metastases. Eur Radiol 2019;29:5844-51.
22. Conte GM, Altabella L, Castellano A, et al. Comparison of T1 mapping and fixed T1 method for dynamic contrast-enhanced MRI perfusion in brain gliomas. Eur Radiol 2019;29:3467-79.
23. Adams LC, Jurmeister P, Ralla B, et al. Assessment of the extracellular volume fraction for the grading of clear cell renal cell carcinoma: first results and histopathological findings. Eur Radiol 2019;29:5832-43.
24. Zhu L, Lai Y, Makowski M, et al. Native T1 mapping of autoimmune pancreatitis as a quantitative outcome surrogate. Eur Radiol 2019;29:4436-46.
25. Endo K, Takahata M, Sugimori H, et al. Magnetic resonance imaging T1 and T2 mapping provide complementary information on the bone mineral density regarding cancellous bone strength in the femoral head of postmenopausal women with osteoarthritis. Clin Biomech (Bristol, Avon) 2019;65:13-8.
26. Alamidi DF, Smailagic A, Bidar AW, et al. Variable flip angle 3D ultrashort echo time (UTE) T1 mapping of mouse lung: A repeatability assessment. J Magn Reson Imaging 2018. [Epub ahead of print].
27. Bruegel M, Gaa J, Woertler K, et al. MRI of the lung: value of different turbo spin-echo, single-shot turbo spin-echo, and 3D gradient-echo pulse sequences for the

detection of pulmonary metastases. J Magn Reson Imaging 2007;25:73-81.
28. Frericks BB, Meyer BC, Martus P, et al. MRI of the thorax during whole-body MRI: evaluation of different MR sequences and comparison to thoracic multidetector computed tomography (MDCT). J Magn Reson Imaging 2008;27:538-45.
29. Dang S, Gao X, Ma G, et al. Combination of free-breathing radial 3D fat-suppressed T1-weighted gradient-echo sequence with diffusion weighted images: Potential for differentiating malignant from benign peripheral solid pulmonary masses. Magn Reson Imaging 2019;57:271-6.
30. Chandarana H, Block TK, Rosenkrantz AB, et al. Free-breathing radial 3D fat-suppressed T1-weighted gradient echo sequence: a viable alternative for contrast-enhanced liver imaging in patients unable to suspend respiration. Invest Radiol 2011;46:648-53.
31. Chandarana H, Block KT, Winfeld MJ, et al. Free-breathing contrast-enhanced T1-weighted gradient-echo imaging with radial k-space sampling for paediatric abdominopelvic MRI. Eur Radiol 2014;24:320-6.
32. Zhang F, Qu J, Zhang H, et al. Preoperative T Staging of Potentially Resectable Esophageal Cancer:A Comparison between Free-Breathing Radial VIBE and Breath-Hold Cartesian VIBE, with Histopathological Correlation. Transl Oncol 2017;10:324-31.
33. Darge K, Anupindi SA, Jaramillo D. MR imaging of the abdomen and pelvis in infants, children, and adolescents. Radiology 2011;261:12-29.

Cite this article as: Yang S, Shan F, Yan Q, Shen J, Ye P, Zhang Z, Shi Y, Zhang R. A pilot study of native T1-mapping for focal pulmonary lesions in 3.0 T magnetic resonance imaging: size estimation and differential diagnosis. J Thorac Dis 2020;12(5):2517-2528. doi: 10.21037/jtd.2020.03.42